

## OSCILLATIONS OF MHD SHOCK WAVES ON THE SURFACES OF T TAURI STARS

A.V. KOLDOBA

Institute of Mathematical Modelling, Russian Academy of Sciences, Moscow, Russia; koldoba@rambler.ru

G.V. USTYUGOVA

Keldysh Institute of Applied Mathematics, Russian Academy of Sciences, Moscow, Russia; ustyugg@rambler.ru

M. M. ROMANOVA

Department of Astronomy, Cornell University, Ithaca, NY 14853-6801; romanova@astro.cornell.edu

R. V.E. LOVELACE

Department of Astronomy and Applied and Engineering Physics, Cornell University, Ithaca, NY 14853-6801; RVL1@cornell.edu

*Draft version November 14, 2018*

### ABSTRACT

This work treats the matter deceleration in a magnetohydrodynamics radiative shock wave at the surface of a star. The problem is relevant to classical T Tauri stars where infalling matter is channeled along the star’s magnetic field and stopped in the dense layers of photosphere. A significant new aspect of the present work is that the magnetic field has an arbitrary angle with respect to the normal to the star’s surface. We consider the limit where the magnetic field at the surface of the star is not very strong in the sense that the inflow is super Alfvénic. In this limit the initial deceleration and heating of plasma (at the entrance to the cooling zone) occurs in a fast magnetohydrodynamic shock wave. To calculate the intensity of radiative losses we use “real” and “power-law” radiative functions. We determine the stability/instability of the radiative shock wave as a function of parameters of the incoming flow: velocity, strength of the magnetic field, and its inclination to the surface of the star. In a number of simulation runs with the “real” radiative function, we find a simple criterion for stability of the radiative shock wave. For a wide range of parameters, the periods of oscillation of the shock wave are of the order 0.02 – 0.2 s.

*Subject headings:* s

tars: magnetic fields — stars: oscillations — MHD — accretion — shock waves — instabilities

### 1. OVERVIEW OF THE PROBLEM

In classical T Tauri stars (CTTSs) matter accretes from the disk to a star through magnetospheric funnel streams (Camenzind 1990; Königl 1991; see also recent review by Bouvier et al. 2007). Similar type accretion but at smaller scales is expected to a magnetized white dwarf (e.g., Warner 1995) and magnetized neutron stars (e.g., Ghosh & Lamb 1979). In the funnel stream, matter is lifted above the equatorial plane and falls down onto the star due to the gravitational acceleration. Large-scale magnetospheric flow has been recently investigated in 2D magnetohydrodynamic (MHD) simulations (Romanova et al. 2002; Bessolaz et al. 2008) and in full 3D MHD simulations (Romanova et al. 2003, 2004; Kulkarni & Romanova 2005). Many aspects of the global magnetospheric flow are now understood. However, interaction of the funnel streams with the surface of the star has not been adequately investigated.

Theoretical models indicate that close to a star matter in the funnel streams is accelerated to almost free-fall velocity, before it hits the high-density layers of the stellar atmosphere. The matter rapidly slows down, forming a shock wave close to the stellar surface. Most of the energy of the flow is radiated behind the shock wave (e.g., Lamzin 1995, 1998; Muzerolle et al. 1998; Calvet & Gullbring 1998; Gullbring et al. 2000; Ardila & Basri 2000). In the case of CTTSs most of energy is radiated in the ultraviolet and soft X-ray bands (e.g., Calvet & Gullbring

1998; Günther & Schmitt 2008). The 3D MHD simulations of magnetospheric flow have show that the hot spots are inhomogeneous and are expected to have higher temperature in the central regions of spots compared to peripheral regions (Romanova et al. 2004). This may have a number of important consequences for investigation of hot spots including the dependence of the filling factor on the wavelength.

If star’s magnetic field of the star is *strong*, then close to the stellar surface the magnetic energy-density is larger than that the kinetic energy-density of the matter. Consequently the matter is passively channeled along the field lines. In this sub-Alfvénic regime a hydrodynamic approach is usually adopted for modeling the shock waves (see §2). The shock wave is found to be non-stationary. It *oscillates* with a high frequency due to the competition between accretion heating in the shock front and radiative cooling behind the front (Langer, Chanmugan & Shaviv 1981; Chevalier & Imamura 1982). If the magnetic field is not very strong near the surface of the star then the flow may be super-Alfvénic. In this regime the orientation of the magnetic field may influence stability of the shock. Only the special case of the flow perpendicular to the magnetic field has been considered so far. It is know that this transverse magnetic field can suppress instability of the shock wave (Smith 1989; Toth & Draine 1993). In this paper we investigate the stability of the radiative shock waves in the super-Alfvénic regime for different ori-

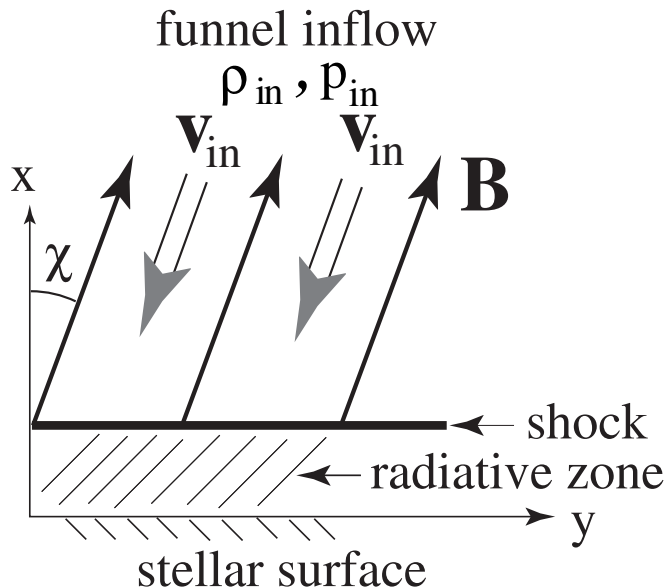


FIG. 1.— Sketch of the geometry of the flow. Matter with density  $\rho_{\text{in}}$  and pressure  $p_{\text{in}}$  flows towards the star with velocity  $v_{\text{in}}$  along the magnetic field which has strength  $B_{\text{in}}$  and is inclined relative to the normal to the surface of the star  $x$  at an angle  $\chi$ . Matter slows down in the MHD shock wave close to the surface of the star and radiates and cools down in the “cooling zone”. Matter may have different angle relative to the field, but we consider the coordinate system in which vectors velocity and magnetic field are parallel to each other.

entations of the magnetic field relative to stellar surface. We consider small patch of the hot spot and investigate the stability of the radiative MHD shock wave for parameters typical for CTTs. Figure 1 shows a sketch of the considered geometry.

For CTTs the expected periods of the oscillations of the shock are very short. The periods vary between 0.02 and 0.2 seconds depending on the parameters. Oscillations in this period range have not been observed so far. Smith, Jones & Clarke (1996) searched for rapid photometric variability in several CTTs in the range of periods from minutes to hours and did not find oscillations. Much higher temporal resolution is required to resolve the oscillations discussed in this paper.

Section 2 of this paper discusses the earlier research on radiative shocks. Section 3 discusses the model and basic equations, and Section 4 the dimensionless variables and scalings. Section 5 comments on the dimensionless variables and the scalings of different quantities, and also describes the stationary structure of the shock. Section 6 discusses the methods used to study the time-dependent shocks, and Section 7 gives our results. Section 8 gives the conclusions of this work.

## 2. EARLIER RESEARCH OF RADIATIVE SHOCKS AND RADIATIVE COOLING FUNCTION

The stability of shock waves has been investigated by different groups both analytically (linear analysis) and numerically. Most of the investigations have been restricted to a *purely hydrodynamic analysis*, because in many situations matter is channeled along the field lines and the problem can be considered as non-magnetic.

First results on interaction of the funnel streams with a star and cooling in the radiative shock wave have been ob-

tained in application to accreting white dwarfs. Numerical modeling of radiative shock wave at the surface of white dwarf led to discovery of instability which is driven by alternation of accreting heating in the shock wave and radiative cooling behind the shock wave and in resulting oscillations of the position of the shock front (Langer, Chamugan & Shaviv 1981). Linear analysis of the stability of a one-dimensional radiative shock wave was done by Chevalier & Imamura (1982). These authors assumed that the radiative cooling from a unit volume is  $\rho^2 T^\alpha$ , and they studied the stability as a function  $\alpha$ . In a more general form the problem has been investigated by Ramachandran & Smith (2004). This work assumed that the radiative losses vary as  $\rho^\beta T^\alpha$ . The boundaries of the stable and unstable regions were found as well as the frequencies and growth rates of the lowest frequency modes for different values of  $\alpha$ ,  $\beta$ . Ramachandran & Smith (2006) investigated the influence of the Mach number of the inflowing gas to the stability of the radiative shock wave. In addition they considered flow at different adiabatic indices  $\gamma$  typical for astrophysical applications and two types of the boundary conditions at the “wall” where the flow is stopped. The influence of boundary conditions on the stability of radiative shock waves has been investigated in detail by Saxton (2002).

A detailed investigation of the linear and nonlinear evolution of one-dimensional radiative shock waves has been done by Mignone (2005, see also Toth & Draine 1993). The intensity of the radiative losses was taken to be  $\rho^2 T^\alpha$ . The stability has been investigated in the linear approximation for the first eight low-frequency modes and it has been established, that: (1) The first eight modes are stable for  $\alpha > 0.92$ ; (2) The fundamental mode ( $n = 0$ ) becomes unstable for  $\alpha < 0.388$ , the  $n = 1$  mode for  $\alpha < 0.782$ ;

(3) In the unstable regime the growth rate is larger for larger mode numbers, but the growth rate of the higher- $n$  modes is not very different from the growth rate of the  $n = 7$  mode; (4) The normalized frequencies of the corresponding modes have an approximately linear dependence on  $n$ , that is,  $\omega_n(\alpha) = \omega_0(\alpha) + n\Delta\omega(\alpha)$ , and decrease as  $\alpha$  increases (excluding the fundamental mode  $n = 0$ ).

The stability of a radiative shock wave in the presence of a *magnetic field* was investigated by Smith (1989). A more detailed investigation of the shock stability in presence of a magnetic field was done by Toth & Draine (1993; hereafter TD93). For the situation considered, the matter flows onto the shock wave perpendicular to its front and the magnetic field has only component parallel to the front. It was concluded that even a modest magnetic field may lead to stabilization of a radiative shock wave which is unstable in the hydrodynamic limit. The higher the harmonic number, the larger the value of the magnetic field which is needed for stabilization of the front for a fixed value of  $\alpha$ . First of all, the magnetic field stabilizes the fundamental mode. In particular, for  $\alpha = -0.5$  the fundamental mode is stabilized at  $M_A^{-1} = [(B_y/\sqrt{4\pi\rho})/v]_{in} = 0.15$ , while the higher modes are stabilized at  $M_A^{-1} = 0.5$ , where  $v$  is velocity of the incoming flow and  $B_y$  is magnetic field parallel to the front.

The subsequent investigation of the stability of the radiative shocks with transversal magnetic field has been done by Ramachandran & Smith, (2005; hereafter RS05). They considered different values of  $\alpha$ ,  $\beta$  in the dependence of the radiative losses, different values  $\gamma$  for the adiabatic index, and also different Mach numbers in the inflowing matter. They obtained new results, and also rederived accurately results by TD93 for the case where  $\gamma = 5/3$  and  $\beta = 2$ .

These earlier studies show that the stability of radiative shock waves depends strongly on the functional dependence of the radiative cooling. In the present work we consider  $\beta = 2$  and a monatomic gas with  $\gamma = 5/3$ . We investigate the stability of the radiative shock waves using a “real” radiative loss function. We calculate this “real” function and approximate it with the power laws. We assume that there is collisional ionization equilibrium (CIE). In this approximation photons freely escape the plasma. Thus, full thermodynamic equilibrium is not established, and the Saha’s formula (for calculation of the degree of the ionization) is not applicable (e.g., Spitzer 1968). The radiative losses under these conditions have been calculated by a number of authors. In these calculations the abundances of the elements are assumed to be Solar. In the paper by Rosner, Tucker, & Vaiana (1978; hereafter RTV) based on the calculations of Raymond & Smith (1977), the radiative losses in the temperature interval  $10^{4.3}\text{K} < T < 10^7\text{K}$  are  $n_e n_H \Lambda(T)$ , where  $n_e, n_H$  are electron density and hydrogen density (total), while the radiation function  $\Lambda(T)$  has been approximated by a multi-segmented power-law (see below). Subsequently,  $\Lambda(T)$  was been calculated at the interval  $10^{3.65}\text{K} < T < 10^8\text{K}$  (Peres et al, 1982). We refer to this function as the “real” cooling

function and add a subscript *RTV*. The dependence is

$$\Lambda_{\text{RTV}}(T) = \begin{cases} (10^{-7.85}T)^{6.15} & 10^{3.9}\text{K} < T < 10^{4.3}\text{K} \\ 10^{-21.85} & 10^{4.3}\text{K} < T < 10^{4.6}\text{K} \\ 10^{-31}T^2 & 10^{4.6}\text{K} < T < 10^{4.9}\text{K} \\ 10^{-21.2} & 10^{4.9}\text{K} < T < 10^{5.4}\text{K} \\ 10^{-10.4}T^{-2} & 10^{5.4}\text{K} < T < 10^{5.75}\text{K} \\ 10^{-21.94} & 10^{5.75}\text{K} < T < 10^{6.3}\text{K} \\ 10^{-17.73}T^{-2/3} & 10^{6.3}\text{K} < T < 10^7\text{K} \\ 10^{-18.21}T^{-0.6} & 10^7\text{K} < T < 10^{7.6}\text{K} \end{cases}$$

The most recent results for radiative losses in the CIE-approximation are given by Gnat & Sternberg (2007; hereafter GS07). In this work it was accepted that the relative abundances of the hydrogen and helium are  $n_{\text{He}}/n_{\text{H}} = 1/12$ . Abundances of other elements (C, Ni, O, N, Mg, Si, S, Fe) are small and they do not give a contribution to the total pressure. However, the intensity of the radiative losses significantly depends on the relative abundance of these elements. For the Solar abundance GS07 proposed an approximation formula:

$$\Lambda_{\text{GS}} = 2.3 \times 10^{-19} T^{-0.54} \text{ erg cm}^3 \text{ s}^{-1}, \quad (1)$$

in the temperature range  $10^5\text{K} < T < 10^8\text{K}$ . The left boundary of this interval corresponds approximately to the maximum of the “real” radiation function which is at  $2.3 \times 10^5\text{K}$ . For temperatures higher than  $6 \times 10^7\text{K}$ , the dominant mechanism of radiative losses is bremsstrahlung radiation with the temperature dependence  $\Lambda \sim \sqrt{T}$ .

According to calculations of GS07 in CIE-approximation, hydrogen is completely ionized for temperature  $T > 3 \times 10^4\text{K}$ , and Helium for  $T > 2 \times 10^5\text{K}$ . Accepting their abundances discussed above we obtain for  $T > 2 \times 10^5\text{K}$ , the electron density  $n_e = n_{\text{H}} + 2n_{\text{He}}$ , and an average mass per particle is  $0.6m_p$ . Thus, the model which we use (based on the CIE-approximation) is applicable for  $T > 2 \times 10^5\text{K}$ . At lower temperatures, the partial ionization of Helium and the change of the average mass per particle become significant. At the temperature  $T = 3 \times 10^4\text{K}$  the fractions of the neutral and ionized atoms of hydrogen and helium are:  $x(\text{H}) = 3.6 \times 10^{-3}$ ,  $x(\text{H}^+) = 0.997$ ,  $x(\text{He}) = 0.4$ ,  $x(\text{He}^+) = 0.6$ ,  $x(\text{He}^{++}) = 0$ . Thus an average mass per particle is  $0.62m_p$ . At a temperature  $T = 2 \times 10^4\text{K}$ , the corresponding fractions are  $x(\text{H}) = 0.078$ ,  $x(\text{H}^+) = 0.922$ ,  $x(\text{He}) = 0.993$ ,  $x(\text{He}^+) = 0.007$ ,  $x(\text{He}^{++}) = 0$ , where an average mass per particle is  $0.66m_p$ . We neglect this factor.

Subsequently we assume that plasma is an ideal gas with equation of state  $p = \mathcal{R}\rho T$  where  $\mathcal{R} = k_B/(0.6m_p) = 1.385 \times 10^8 \text{ erg g}^{-1} \text{ K}^{-1}$  is gas constant.

In the paper GS07 it is shown that for  $T < 10^6\text{K}$ , the radiative losses, calculated in CIE-approximation, exceed losses which occur in non-stationary plasma cooling. This is connected with the fact that in the first case the ionization level of elements participating in the main radiative processes is lower because in the non-stationary regime recombination lags the cooling. However, we use the more detailed approximation mentioned above after changing the normalization.

Figure 2 shows the radiative cooling functions  $\Lambda_{\text{RTV}}(T)$  (thick solid line) and  $\Lambda_{\text{GS}}(T)$  (thin solid line). The diagonal dashed line shows the dependence of the upstream

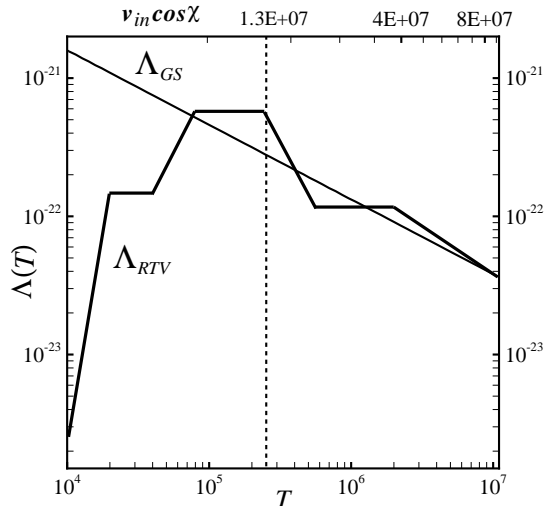


FIG. 2.— Cooling function  $\Lambda_{RTV}(T)$  (thick solid line) and  $\Lambda_{GS}(T)$  (thin solid line) as a function of  $T$  in K. The vertical dotted line shows our illustrative value of velocity before the shock  $v_{in} \cos \chi = 1.3 \times 10^7 \text{ cm s}^{-1}$  and the corresponding temperature behind the shock.

velocity normal to the shock ( $v_{in} \cos \chi$ ) on the temperature behind the shock (for  $\gamma = 5/3, p_{in} = 0$ ):  $T_s = 3(v_{in} \cos \chi)^2 / (16\mathcal{R})$ . The horizontal dashed line shows the velocity of the incoming flow  $v_{in}$  (for illustration of the calculated results we take  $v_{in} \cos \chi = 1.3 \times 10^7 \text{ cm s}^{-1}$ ) and corresponding to this velocity temperature behind the shock wave front.

Section 2 of the paper discusses the model and basic equations, and Section 3 the dimensionless variables and scalings. Section 3 comments on the dimensionless variables and the scalings of different quantities. Section 4 describes the stationary structure of the shock. Section 5 discusses the methods used to study the time-dependent shocks, and Section 6 gives our results. Section 7 gives the conclusions of this work.

### 3. FORMULATION OF THE PROBLEM

We investigate formation and evolution of the shock wave near the surface of the star which forms as a result of disk accretion to a star through a funnel flow. The accreting matter is sufficiently ionized to satisfy the frozen-in condition so that matter of the funnel streams is channeled by the magnetic field and close to the star it flows along the field lines.

Figure 1 shows the geometry. Matter with velocity  $v_{in}$ , density  $\rho_{in}$ , and pressure  $p_{in}$  flows towards the surface of the star along the magnetic field. The magnetic field has a strength  $B_{in}$  and is directed at an angle  $\chi$  relative to the normal vector to the surface of the star  $\hat{\mathbf{x}}$ . The  $x$ -axis is normal to the surface of the star and the  $y$ -axis is tangential to its surface and is directed such that the magnetic field is located in the  $(x, y)$  plane. We neglect small perturbations in  $z$ -direction associated with propagation of the Alfvén waves. We consider that the magnetic field has an arbitrary inclination angle  $\chi$  relative to the normal to the star's surface. In general, the matter flow velocity is not parallel to the magnetic field. However, such parallel orientation can be obtained by transformation of the

coordinate system.

Heating of matter occurs in the front of the MHD shock wave. In the cooling zone behind the shock, matter radiates energy, is decelerated, and become denser up to the moment, when the radiative cooling stops. Formally this happens when  $T = 0$ . The height of the radiative zone is small compared to either width of the funnel stream or to the radius of the star. Thus we can neglect the inhomogeneity of the accretion flow in the  $(y, z)$  directions. (See Canalle et al. 2005 for a discussion of cases where the converging of the field lines is important.) We also neglect small effects associated with acceleration by gravity of the star (considered e.g., by Cropper et al. 1999) because the region we consider is small. Generally, the structure consisting of the shock wave and the cooling zone is unstable to both longitudinal,  $x$ ) perturbations (which can be studied in one-dimensional approach), and to transverse  $(y, z)$  perturbations (Bertschinger 1986; Imamura et al. 1996). The latter makes the problem more than one-dimensional even if the flow is homogeneous. In the present work the spatial perturbations are not considered.

We consider conditions where the star's mass is  $M_* = 0.8M_\odot$  and its radius is  $R_* = 2R_\odot$ . In this case the free-fall speed at the star's surface is  $v_{ff} = \sqrt{2GM_*/R_*} = 4 \times 10^7 \text{ cm s}^{-1}$ . If the temperature of accreting matter is  $10^4 \text{ K}$ , then the sound speed is  $2 \times 10^6 \text{ cm s}^{-1}$  (for average mass per particle  $0.6m_p$ ). Clearly, the accretion is strongly supersonic; the sonic Mach number is 20. For a surface magnetic field  $B = 10^3 \text{ G}$  and density of the inflowing matter  $10^{-11} \text{ g cm}^{-3}$  (Romanova et al. 2002), the Alfvén velocity is  $c_A = B/\sqrt{4\pi\rho} = 10^8 \text{ cm s}^{-1}$ . For these parameters the flow is sub-Alfvénic. However, for  $B < 3 \times 10^2 \text{ G}$  and the other parameters the same the flow is super-Alfvénic and perturbations from the shock wave cannot propagate up the stream. Strictly speaking we should compare the velocity of the accreting matter with the fast magnetosonic velocity, but it does not differ significantly from the Alfvén velocity because the sound

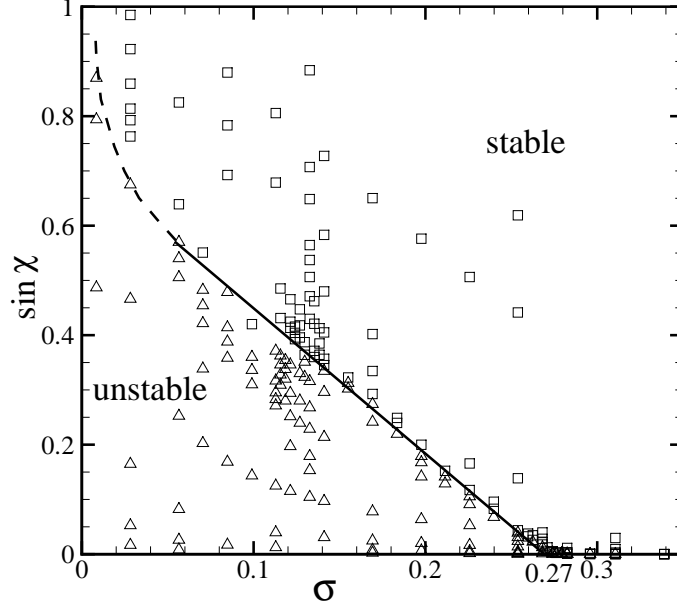


FIG. 3.— The position of the boundary between stable and unstable radiative shock waves as a function of parameters  $(\sigma, \sin \chi)$  for a velocity of accretion  $v_{\text{in}} \cos \chi = 1.3 \times 10^7 \text{ cm s}^{-1}$ .

speed is small. Thus, both cases are interesting: stability of the radiative shock waves for sub-Alfvénic and super-Alfvénic inflows. However, we restrict the present study to super-Alfvénic inflow.

We assume that the radiation zone behind the shock is optically thin in the direction perpendicular to the star’s surface and to the front of the shock wave. The dominant radiation loss mechanisms are determined by the “thermodynamic” state of plasma. We assume that the state of the matter can be described in terms of a temperature which is the same for the ions and electrons. For the considered conditions, the radiative losses per unit volume is  $\rho^2 \Lambda(T)$ , where  $\rho$  is the plasma density and  $\Lambda(T)$  is the radiative function obtained from  $\Lambda_{\text{RTV}}(T)$  or from  $\Lambda_{\text{GS}}(T)$  by renormalization. We consider that the accreting matter is an ideal gas with adiabatic index  $\gamma = 5/3$  both before the compression at the shock front and in the radiation zone.

In the absence of the magnetic field, and when the matter falls perpendicular to the surface of the star, the temperature behind the shock is  $T = 10^5 v_7^2 \text{ K}$ , where  $v_7 = v/(10^7 \text{ cm s}^{-1})$ , and the average mass per particle is  $0.6 m_p$ . For velocities of the incoming matter  $v = 4 \times 10^7 \text{ cm s}^{-1}$ , the temperature behind the shock reaches  $1.6 \times 10^6 \text{ K}$ . At such temperature both hydrogen and helium atoms are completely ionized according to the CIE approximation.

We consider the situation where the matter accretes to the star along magnetic field lines inclined by an angle  $\chi$  to the normal to the star’s surface. The shock is parallel to the star’s surface and it remains parallel as it moves. That is, we consider variations only in the  $x$ -direction. The equations describing this situation are following:

$$\frac{\partial \rho}{\partial t} + \frac{\partial(\rho v_x)}{\partial x} = 0 ,$$

$$\frac{\partial(\rho v_x)}{\partial t} + \frac{\partial}{\partial x} \left( \rho v_x^2 + p + \frac{B_y^2}{8\pi} \right) = 0 ,$$

$$\frac{\partial(\rho v_y)}{\partial t} + \frac{\partial}{\partial x} \left( \rho v_x v_y - \frac{B_x B_y}{4\pi} \right) = 0 ,$$

$$B_x = \text{const} ,$$

$$\frac{\partial B_y}{\partial t} + \frac{\partial}{\partial x} (v_x B_y - v_y B_x) = 0 ,$$

$$\frac{\partial}{\partial t} \left( \frac{\rho v^2}{2} + \frac{p}{\gamma - 1} + \frac{B^2}{8\pi} \right)$$

$$+ \frac{\partial}{\partial x} \left[ v_x \left( \frac{\rho v^2}{2} + \frac{\gamma p}{\gamma - 1} \right) + \frac{B_y}{4\pi} (v_x B_y - v_y B_x) \right] = -\rho^2 \Lambda(T) . \quad (2)$$

Here  $v^2 \equiv v_x^2 + v_y^2$ ,  $B^2 \equiv B_x^2 + B_y^2$ . In the unperturbed flow upstream of the shock,

$$B_x = B_{\text{in}} \cos \chi , \quad B_y = B_{\text{in}} \sin \chi ,$$

$$v_x = -v_{\text{in}} \cos \chi , \quad v_y = -v_{\text{in}} \sin \chi ,$$

$$\rho = \rho_{\text{in}} , \quad p = p_{\text{in}} .$$

We consider that the pressure in the incoming flow is very small so that it does not influence the MHD-shock wave and cooling zone. Equivalently, the sonic Mach number is

much larger than unity. As discussed earlier, we choose a coordinate system in which the flow velocity and magnetic field are both in the  $(x, y)$  plane.

In contrast with the non-magnetic case (TD93), the density  $\rho$  does not increase unrestrictedly at the right-hand boundary of the radiative zone and correspondingly the velocity  $v_x$  does not approach zero. Here, the temperature  $T = p/(\mathcal{R}\rho)$  may approach zero not because  $\rho \rightarrow \text{inf}$  but because  $p \rightarrow 0$ . At the same time the total, gas plus magnetic field pressure remains constant. In the cooling zone the accreting matter does not reach zero flow speed. Thus, the radiative shock provides only part of the deceleration and absorption of matter by the magnetized star.

Our treatment of the stability of the radiative MHD shock wave is different in essential respects from that of TD93 and RS05. In these papers the magnetic field is transverse to the flow and parallel to the star's surface,  $\mathbf{B} = B_y \hat{\mathbf{y}}$ . We neglect the difference in cooling laws and adiabatic index  $\gamma$  (RS05) which are not significant. To approach this case in our model, we need to take  $\chi \rightarrow \pi/2$ , and parameters in the incoming flow  $v_x = -v_{\text{in}} \cos \chi$ ,  $B_y = B_{\text{in}} \sin \chi \rightarrow B_{\text{in}}$ . The Alfvénic Mach number is

$$M_A = \frac{v_{\text{in}} \cos \chi}{B_{\text{in}}/\sqrt{4\pi\rho_{\text{in}}}} = \frac{\cos \chi}{\sigma}. \quad (3)$$

To have  $M_A$  a fixed value as  $\chi \rightarrow \pi/2$ , we let  $\sigma \equiv \cos \chi/M_A$  and require

$$B_x = B_{\text{in}} \cos \chi \rightarrow 0, \quad v_x \rightarrow -M_A \frac{B_{\text{in}}}{\sqrt{4\pi\rho_{\text{in}}}},$$

$$v_y = -M_A \tan \chi \frac{B_{\text{in}}}{\sqrt{4\pi\rho_{\text{in}}}} \rightarrow \infty.$$

A tangential velocity  $v_y$  can be included in the calculations of TD93 by a Galilean transformation to another reference frame. Thus, a radiative MHD shock wave with the magnetic field parallel to the star's surface and perpendicular to the flow corresponds to the limit where  $\chi \rightarrow \pi/2$  and  $\sigma = \cos \chi/M_A \rightarrow 0$ .

#### 4. DIMENSIONLESS VARIABLES AND SCALINGS

Consider firstly the case where the radiation function is a power law,  $\Lambda(T) = A(\mathcal{R}T)^\alpha$ , where  $\mathcal{R}$  is the gas constant. The coefficient  $A$  has dimension  $\text{cm}^{5-3\alpha} \text{g}^{-1} \text{s}^{\alpha-3}$ . For estimates we assume that the hydrogen and helium are completely ionized and that the average mass per particle is  $0.6m_p$ . In the paper GS07 the radiative energy losses per unit of volume are given in the form of equation (1). With these simplifications and renormalization,

$$\Lambda_{\text{GS}} = 1.37 \times 10^{32} (\mathcal{R}T/\text{cm}^2 \text{s}^{-2})^{-0.54} \text{cm}^5 \text{g}^{-1} \text{s}^{-3}.$$

We rewrite our equations in dimensionless form choosing fiducial dimensional values for the main variables and introducing dimensionless variables  $\hat{A} = A/A_0$  for different variables  $A$ . The fiducial values are taken to be: For the velocity,  $v_0 = v_{\text{in}} \cos \chi$ ; for the density,  $\rho_0 = \rho_{\text{in}}$ ; for the distance,  $v_0^{3-2\alpha}/A\rho_0$ ; for time,  $v_0^{2-2\alpha}/(A\rho_0)$ ; for the pressure,  $\rho_0 v_0^2$ ; for the magnetic field,  $v_0 \sqrt{\rho_0}$ ; and for the temperature  $v_0^2/\mathcal{R}$ . In dimensionless variables, the system of

equations has the same form. Subsequently we remove tilde signs from dimensionless variables. The formula for the radiative losses now has the form  $\rho^2 T^\alpha$ , while in the incoming flow  $v_{\text{in}} \cos \chi = -1$ ,  $\rho_{\text{in}} = 1$ ,  $B_{\text{in}} = \sigma \sqrt{4\pi}$ ,  $p_{\text{in}} \ll 1$ , where  $\sigma$  is the inverse of the Alfvén Mach number.

It is clear that in power law case,  $\Lambda \sim T^\alpha$ , the stability/instability of the radiative shock in presence of a magnetic field does not depend solely on  $v_{\text{in}}$  and  $B_{\text{in}}$ , but instead on their combination in the form  $(B_{\text{in}}/\sqrt{4\pi\rho_{\text{in}}})/v_{\text{in}} = \sigma = M_A^{-1}$ . Furthermore, the stability criterion does not depend on the coefficient  $A$ . However,  $A$  determines the spatial scale of the radiative zone and the temporal scale for oscillations if they are present.

We chose the spatial scale is  $10^7 v_7^{4.08}/(\rho_{-11}) \text{cm}$  and the time scale is  $v_7^{3.08}/(\rho_{-11}) \text{s}$ , where  $v_7$  is the velocity in units of  $10^7 \text{cm s}^{-1}$  and  $\rho_{-11}$  is the density in units of  $10^{-11} \text{g cm}^{-3}$ . In reality, both estimates are about three orders of magnitude larger than the observed values. Such scales follow from the solution of the equation for the stationary shock wave, where the pressure goes to zero for  $x \gg 1$  (TD93). The same is true for the scale of time. Thus, the height of the cooling zone is in fact  $\sim 10^4 \text{cm}$ , and the periods of oscillation are several hundredths of a second.

We now consider the ‘‘real’’ radiative function (RTV) which is not a power law. This is why strictly speaking the stability condition of radiative shock waves depends not only on  $\sigma$  but also on both  $v_{\text{in}}$  and  $B_{\text{in}}$ . However, over a sufficiently wide range of temperatures, the radiative function can be roughly approximated by a power law of the temperature. This suggests that the stability condition will depend mainly on  $\sigma$  with a weaker dependence on  $v_{\text{in}}$  and  $B_{\text{in}}$ .

#### 5. STATIONARY STRUCTURE

We are interested in the stability of the stationary flow consisting of the MHD shock wave and the downstream radiative zone. The stationary flow is described by

$$\rho v_x = -j = -\rho_{\text{in}} v_{\text{in}} \cos \chi,$$

$$p + \rho v_x^2 + \frac{B_y^2}{8\pi} = q_x = p_{\text{in}} + \rho_{\text{in}} v_{\text{in}}^2 \cos^2 \chi + \frac{B_{\text{in}}^2}{8\pi} \sin^2 \chi,$$

$$\rho v_x v_y - \frac{B_x B_y}{4\pi} = q_y = \left( \rho_{\text{in}} v_{\text{in}}^2 - \frac{B_{\text{in}}^2}{4\pi} \right) \sin \chi \cos \chi,$$

$$v_x B_y - v_y B_x = 0,$$

$$j \frac{d}{dx} \left( \frac{v^2}{2} + \frac{\gamma p / \rho}{\gamma - 1} \right) = \rho^2 \Lambda. \quad (4)$$

In the last equation there is no term describing the energy flux of the electromagnetic field, because the Poynting flux in our coordinate system is zero ( $\mathbf{E} = -\mathbf{v} \times \mathbf{B}/c = 0$ ).

The stationary structure of the shock wave and radiative zone is described by the following equation for specific volume  $V$ ,

$$\frac{dV}{dx} = \frac{\Lambda(T)}{jV^2 F(V)}, \quad (5)$$

$N$	<i>cooling function</i>	$v_{in} \cos \chi$ cm s <sup>-1</sup>	$\sin \chi$	$B_{in}$ (G)	<i>stab/unstab</i>
<i>I</i>	<i>RTV</i>	$1.3 \times 10^7$	0.154	40.8	<i>unst</i>
<i>II</i>	<i>GS</i>	$1.3 \times 10^7$	0.154	40.8	<i>unst</i>
<i>III</i>	<i>RTV</i>	$3 \times 10^7$	0.154	94.9	<i>unst</i>
<i>IV</i>	<i>RTV</i>	$1.3 \times 10^7$	0.368	36.4	<i>stab</i>

TABLE 1

The Table shows parameters used in our main runs.

where

$$F(V) = j^2 V \left[ 1 + \frac{q_y^2 B_x^2 / 4\pi}{(B_x^2 / 4\pi - j^2 V)^3} \right] + \quad (6)$$

$$\frac{\gamma}{\gamma + 1} \left[ q_x - 2j^2 V - \frac{q_y^2 B_x^2 / 8\pi}{(B_x^2 / 4\pi - j^2 V)^3} \left( j^2 V + \frac{B_x^2}{4\pi} \right) \right].$$

The other variables are determined from equations (4). In particular,

$$v_x = -jV, \quad B_y = -\frac{B_x q_y}{B_x^2 / 4\pi - j^2 V},$$

$$v_y = \frac{B_y}{B_x} v_x = \frac{q_y jV}{B_x^2 / 4\pi - j^2 V},$$

$$p = q_x - j^2 V - \frac{q_y^2 B_x^2 / 8\pi}{(B_x^2 / 4\pi - j^2 V)^2}, \quad T = \frac{pV}{\mathcal{R}}. \quad (7)$$

As mentioned we investigate stability of the structure “fast MHD shock wave” plus “cooling zone”. Note that as the angle  $\chi$  between the flow velocity and the normal to the shock is decreased, the stationary MHD structure does not convert to the hydrodynamic one. In the limit  $\chi \rightarrow 0$ ,  $q_x \approx B_x^2 / (4\pi\sigma^2)$ . The pressure in the radiative zone is determined from the relation

$$p \approx \frac{B_x^2}{4\pi\sigma^2} - j^2 V - \frac{q_y^2 B_x^2 / 8\pi}{(B_x^2 / 4\pi - j^2 V)^2}, \quad (8)$$

where  $q_y \propto \sin \chi$  is small. For the considered conditions where  $\sigma < 1$ , the denominator of the fraction of the last term goes to zero before the  $B_x^2 / (4\pi\sigma^2) - j^2 V$  goes to zero. Thus the pressure goes to zero for  $B_x^2 / 4\pi - j^2 V \approx 0$ . That is, the velocity of the flow at the exit from the radiative zone approaches the Alfvén velocity and is  $v_x \approx -B_x^2 / (4\pi j)$ . Taking into account equation (7), we obtain from equation (8),

$$0 \approx \frac{B_x^2}{4\pi\sigma^2} - \frac{B_x^2}{4\pi} - \frac{B_x^2}{8\pi} \left( \frac{v_y}{B_x^2 / 4\pi j} \right)^2. \quad (9)$$

From this relation we obtain

$$v_y \approx -B_x \sqrt{\frac{1 - \sigma^2}{2\pi\rho_{in}}}, \quad B_y \approx \frac{B_x}{\sigma} \sqrt{2(1 - \sigma^2)}. \quad (10)$$

Thus, as  $\chi \rightarrow 0$  the components of the velocity and magnetic field parallel to the shock approach finite values. In contrast, in the gas dynamic case these components approach zero. The observed behavior is similar to that known to occur in MHD switch-on shock waves where finite tangential velocity and magnetic field components are generated, and where the velocity of the flow behind the front is Alfvénic (Smith, 1993). Note that the parallel MHD shock wave becomes non-evolutionary, and it is replaced by a switch-on shock wave for  $[v_x / (B_x / \sqrt{4\pi\rho})]_{in} < 2$  for  $\gamma = 5/3$  and  $p_{in} = 0$ .

## 6. METHOD

We study the stability/instability of radiative shock waves in the presence of the magnetic field by integrating the time-dependent one-dimensional MHD equations in a region containing the shock and the radiative cooling zone. We used an Eulerian variables. Consequently, the simulation region is chosen large enough to contain both the shock wave and the remote part of the radiative zone where energy losses are negligibly small. The location of the right-hand boundary of the simulation region is chosen so that the shock wave did not leave the region during oscillations. For the calculations of the MHD flows we used a high resolution Godunov type numerical scheme (see, e.g., Kulikovskii, Pogorelov & Semenov 2000).

For initial conditions we take the stationary flow with the shock wave and the radiation zone. At the top of the simulation region (see Figure 1) we determined either parameters of unperturbed flow (density, velocity, etc.) if the incoming flow is super-Alfvénic, or we had “free” boundary conditions, if incoming flow is sub-Alfvénic.

At the bottom of the simulation region (closer to stellar surface), we have a “layer” with no radiative losses. At this boundary we fixed the longitudinal velocity at a small value corresponding to the stationary solution. All other variables at the boundary had the same value as in the previous cell. Simulations have shown that results of modeling are not sensitive to the boundary conditions on the transverse components of velocity and magnetic field. At the boundary cell the density varied around some average value and the mass did not accumulate there. For example in case I the sound speed in this cell has been  $(1-3) \times 10^6$  cm s<sup>-1</sup>, the size of the grid = 81cm, the sound-crossing time  $< 10^{-4}$ s. We observed from simulations that variation of this boundary did not influence much to the oscillations.

The spatial resolution has been chosen so that the radiation zone is covered by 200 cells. The size of the simulation

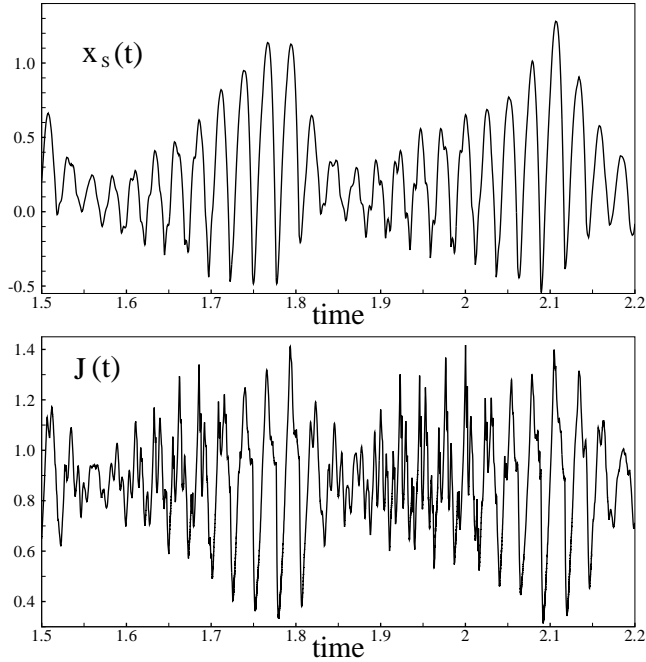


FIG. 4.— Time dependence of the shock front coordinate  $x_s$  (top panel) and luminosity  $J$  (bottom panel) for case I (“real” cooling function,  $v_{\text{in}} \cos \chi = 1.3 \times 10^7 \text{cm s}^{-1}$ ). The shock front coordinate is in units  $\Delta$ , luminosity in units of  $J_{\text{in}}$ , and time is in seconds.

region has been chosen such that during the oscillations the shock wave stayed inside the simulation region. Depending on the amplitude of oscillations the simulation region incorporated from 500 to 1,500 cells. The time-step has

been chosen automatically such that the Courant number is 0.5.

## 7. RESULTS

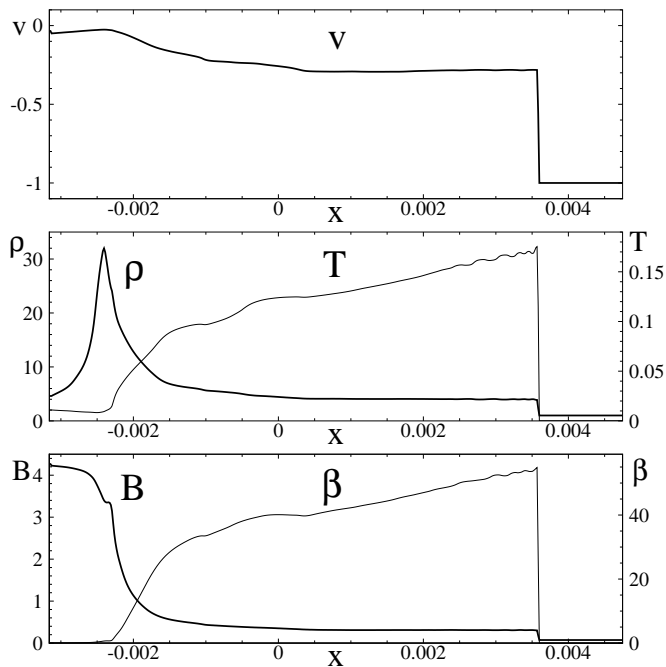


FIG. 5.— Distribution of different parameters along the  $x$ -axis: velocity component along the field lines (top panel), density and temperature (middle panel), magnetic field and plasma parameter  $\beta$  (low panel). All variables are shown in dimensionless form. In the incoming flow  $v_x = -1$ ,  $\rho = 1$ ,  $T = 0$  (almost zero),  $B_x = 0.48$ ,  $B_y = 0.076$ . Matter inflows from the right boundary, a star is at the left.



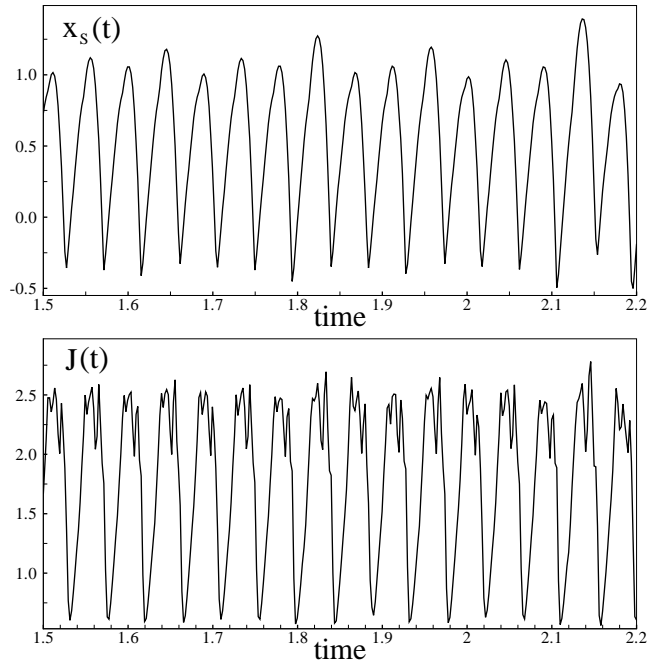


FIG. 6.— Time dependence of shock front coordinate  $x_s$  (top panel) and luminosity  $J$  (bottom panel) for case II (power-law cooling function,  $v_{\text{in}} \cos \chi = 1.3 \times 10^7 \text{ cm s}^{-1}$ ). The coordinate of the shock front  $x_s$  is in units  $\Delta$ , the luminosity is in units of  $J_{\text{in}}$ , and the time is in seconds.

We investigate the stability/instability of the radiative shock wave as a function of two main dimensionless parameters: the inverse Alfvén Mach number of the unperturbed upstream flow  $\sigma = M_A^{-1}$  and the inclination angle of the flow,  $\chi$ , relative to the normal to the star’s surface. The

limit  $\sigma = 0$  corresponds to zero magnetic field.

We performed a series of calculations in which we varied these two parameters. Figure 3 summarizes the results. In the plane  $(\sigma, \sin \chi)$  markers show the parameters where calculations were done. The “squares” show the

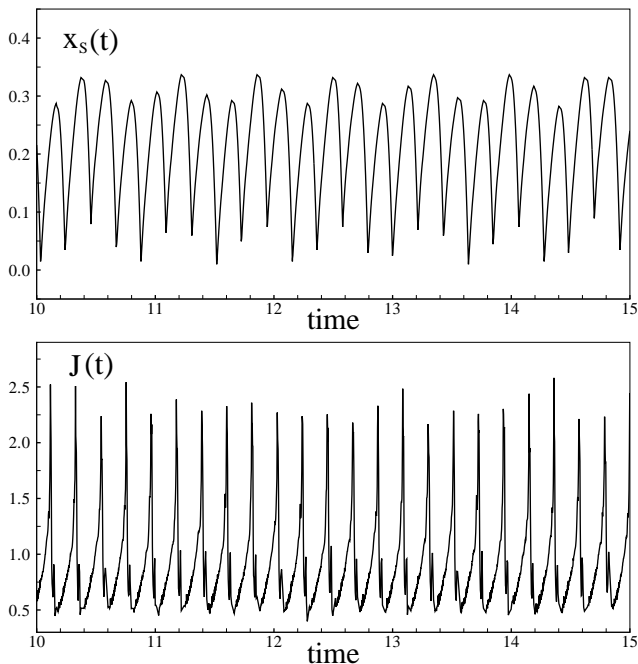


FIG. 7.— Time dependence of the shock front coordinate  $x_s$  (top panel) and luminosity  $J$  (bottom panel) for case III (“real” cooling function,  $v_{\text{in}} \cos \chi = 3 \times 10^7 \text{ cm s}^{-1}$ ). The shock front coordinate is in units  $\Delta$ , the luminosity is in units of  $J_{\text{in}}$ , and the time is in seconds.

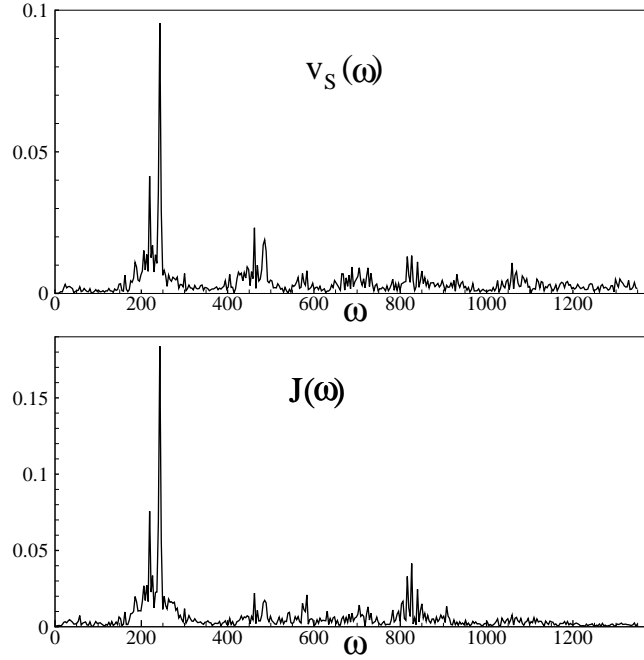


FIG. 8.— Fourier amplitudes of shock front velocity  $v_s$  (top panel) and luminosity  $J$  (bottom panel) for case I. Velocity is in  $v_{\text{in}} \cos \chi$ , luminosity is in  $J_{\text{in}}$ , frequency is in  $\text{s}^{-1}$ .

parameters for which the radiative shock wave is stable and the “triangles” show cases where it is unstable. The solid straight line with a dashed continuation is the stability/instability boundary. The condition for stability can be expressed as

$$3.7\sigma + 1.4 \sin \chi \geq 1, \quad (11)$$

for conditions where the magnetic field is not very weak,  $\sigma \geq 0.02$ .

For weak magnetic fields ( $\sigma \leq 0.02$ ), the boundary of stability is located close to the vertical axis in Figure 3. This part of the boundary is shown as a dashed line. Thus, in the absence of a magnetic field, the radiative shock wave (for the same parameters of the incoming

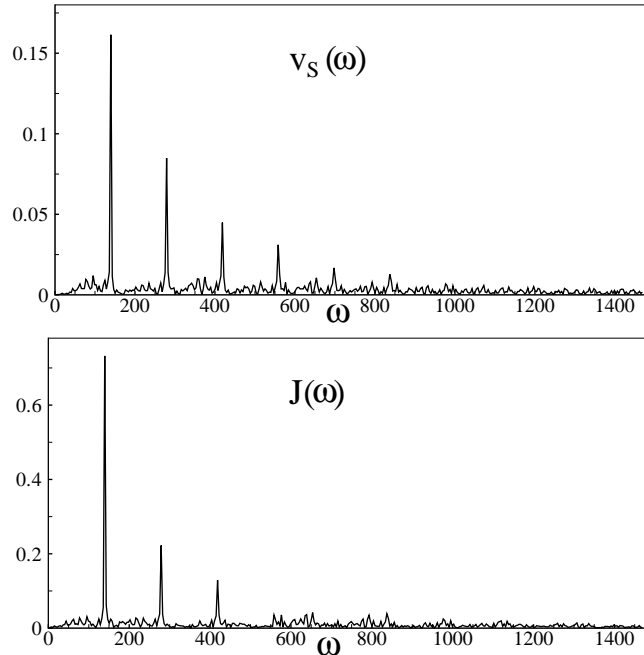


FIG. 9.— Fourier amplitudes of shock front velocity  $v_s$  (top panel) and luminosity  $J$  for case II (cooling function  $\Lambda_{\text{GS}}$ ,  $v_{\text{in}} \cos \chi = 1.3 \times 10^7 \text{cm s}^{-1}$ ). The velocity is in units of  $v_{\text{in}} \cos \chi$ , the luminosity is in units of  $J_{\text{in}}$ , and frequency is in  $\text{s}^{-1}$ .

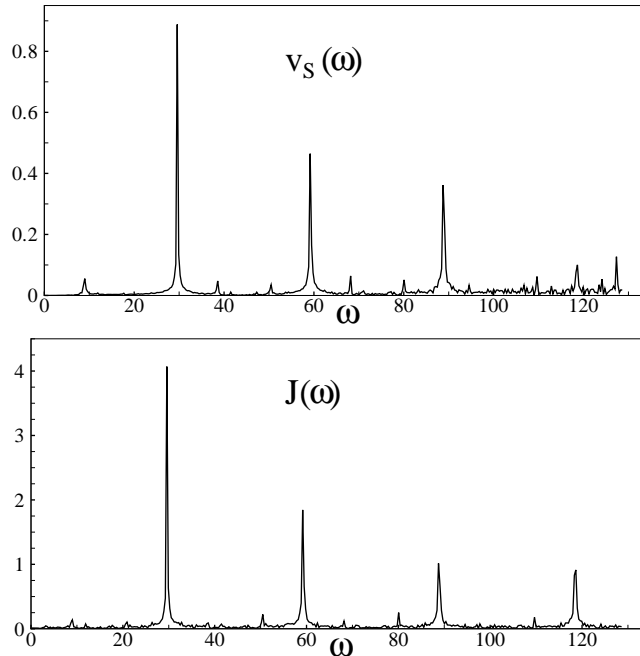


FIG. 10.— Fourier amplitudes of shock front velocity  $v_s$  and luminosity  $J$  for case III (cooling function  $\Lambda_{RTV}$ ,  $v_{\text{in}} \cos \chi = 3 \times 10^7 \text{cm s}^{-1}$ ). The velocity is in units of  $v_{\text{in}} \cos \chi$ , the luminosity is in units of  $J_{\text{in}}$ , and the frequency is in  $\text{s}^{-1}$ .

flow) is unstable. However, even a small magnetic field, in particular, inclined one, stabilizes the radiative shock wave. For  $\sigma \geq 0.02$  ( $M_A \leq 50$ ), we find stability for angles  $\chi > 45^\circ$ . If the magnetic field is sufficiently strong  $\sigma \geq 0.27$  ( $M_A \leq 3.7$ ), then the radiative shock wave is stable for all angles  $\chi$ .

We emphasize again that in the limit of small inclination angles,  $\chi \rightarrow 0$ , our model does not correspond to a gas-dynamical flow with unperturbed magnetic field.

To understand the temporal characteristics of unstable radiative shock waves, we performed calculations using the “real” cooling function  $\Lambda_{RTV}$  and for some cases with the function  $\Lambda_{GS}(T)$ . In all calculations we followed the location of the shock wave  $x_s(t)$  and the total intensity of radiation from the radiative zone per unit area  $J(t) = \int dx \rho^2 \Lambda$ .

Figure 4 shows results of calculation of evolution of the radiative shock wave with radiation function  $\Lambda_{RTV}$

for the following parameters of the incoming flow:  $v_{\text{in}} = 1.3 \times 10^7 \text{cm s}^{-1}$ ,  $\rho_{\text{in}} = 10^{-11} \text{g cm}^{-3}$ ,  $B_{\text{in}} = 40.8 \text{G}$ ,  $\sin \chi = 0.154$ . Also,  $\sigma = 0.13$ . The width of the cooling zone in the stationary regime is  $\Delta \approx 1.64 \times 10^4 \text{cm}$ , and the energy-density (excluding the much smaller thermal energy) is  $J_{\text{in}} = (1/2) \rho_{\text{in}} v_{\text{in}}^3 \cos \chi = 1.07 \times 10^{10} \text{erg cm}^{-2} \text{s}^{-1}$ . We point out once again that the incoming flow velocity is along the magnetic field, so that there is no Poynting flux.

For the mentioned parameters, the stationary shock is unstable and the shock and radiative zone oscillate. The position of the front of the shock wave oscillates with a period  $\approx 0.025 \text{s}$ . The amplitude of oscillations of the front is modulated and varies with period  $\approx 0.3 \text{s}$ . The top panel of Figure 4 shows the position of the front as a function of time at the time-interval approximately equal to twice period of modulation. The bottom panel of Figure 4 shows the temporal variation of the radiation intensity from the radiation zone for the same time-interval as the top panel.

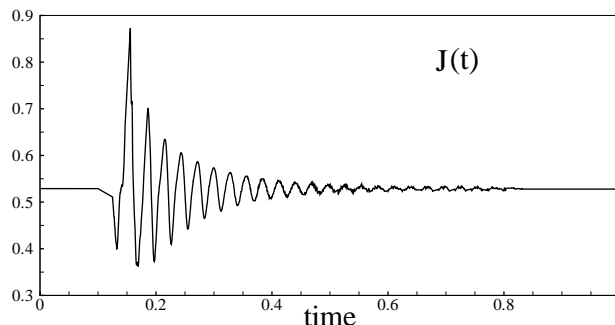


FIG. 11.— Time dependence of luminosity  $J$  for case IV (cooling function  $\Lambda_{RTV}$ ,  $v_{\text{in}} \cos \chi = 1.3 \times 10^7 \text{cm s}^{-1}$ ). The luminosity is in units of  $J_{\text{in}}$ , and the time is in seconds.

The position of the shock front is normalized to the width of the stationary cooling zone  $\Delta$ . The intensity of radiation is normalized to the energy-density in the incoming flow  $J_{\text{in}}$ . The time is in seconds.

Figure 5 shows spatial distribution of the longitudinal ( $x$ -direction) velocity (top panel), density and temperature (middle panel), longitudinal magnetic field and plasma parameter  $\beta = 8\pi p/(B_x^2 + B_y^2)$  (bottom panel) at a time corresponding to the maximum distance of the shock from the surface of the star. In stationary regime the shock wave is located at  $x = 0$ , while the radiative zone is below this. See animations at <http://www.astro.cornell.edu/usrus/shock.htm>

Figure 6 shows results of calculation of the evolution of the radiative shock wave for the same parameters in the incoming flow but with the radiation function  $\Lambda_{\text{GS}}$  (case II). The width of the cooling zone in the stationary regime is  $\Delta \approx 2.65 \times 10^4 \text{cm}$ . This figure shows position of the front of the shock wave  $x_s(t)$  (top panel) and intensity of radiation  $J(t)$  (bottom panel). One can see that qualitatively the oscillations are similar. However, the main frequency of oscillations is different:  $\omega_{\text{RTV}} \approx 240 \text{s}^{-1}$ , whereas  $\omega_{\text{GS}} \approx 140 \text{s}^{-1}$ . With the radiation function  $\Lambda_{\text{GS}}$ , the modulation of the oscillation amplitude of the position of the front is small.

Figure 7 shows results of calculation of evolution of the radiative shock wave with radiation function  $\Lambda_{\text{RTV}}$  for the following parameters of the incoming flow (case III):  $v_{\text{in}} = 3 \times 10^7 \text{cm s}^{-1}$ ,  $\rho_{\text{in}} = 10^{-11} \text{gcm}^{-3}$ ,  $B_{\text{in}} = 94.9 \text{G}$ ,  $\sin \chi = 0.154$ . Also,  $\sigma = 0.13$ . The width of the cooling zone in the stationary regime is  $\Delta \approx 8.86 \times 10^5 \text{cm}$ , and the energy-density (excluding the small thermal energy) is  $1.35 \times 10^{11} \text{erg cm}^{-2} \text{s}^{-1}$ . As in case I for these parameters the stationary shock is unstable and the shock oscillates. The position of the front of the shock wave oscillates with period  $\approx 0.21 \text{s}$ . The top panel shows the position of the front as a function of time, and the bottom panel shows the variation of the radiation intensity for the same time interval as the top panel.

In case III we increased both the velocity and magnetic field with the aim of checking our hypothesis, that the qualitative solution of the problem (while using the “real” radiation function  $\Lambda_{\text{RTV}}$ ) is determined by the dimensionless parameters of the problem,  $\sin \chi$ , and the magnetization,  $\sigma$ , and not by dimensional values of velocity of the incoming flow and the magnetic field.

Figure 8 shows results of the Fourier-analysis of the speed of the shock front and total luminosity per unit of area  $v_s(\omega)$  and  $J(\omega)$ . One can see that when modelling with radiation function  $\Lambda_{\text{RTV}}$  (case I) then two nearby maxima of the Fourier amplitudes are observed at the frequencies  $\omega_1 = 240 \text{s}^{-1}$ ,  $\omega_2 = 260 \text{s}^{-1}$ . We suggest that the combination of these two frequencies gives the amplitude modulation evident in Figure 4.

Figure 9 shows the Fourier amplitudes for case II where we use  $\Lambda_{\text{GS}}$ . The Fourier-amplitudes for both,  $v_s$ , and  $J$  have sharp maxima at frequencies divisible by the main frequency.

Figure 10 shows the Fourier amplitudes for case III where we use  $\Lambda_{\text{RTV}}$ . The Fourier-amplitudes for both,  $v_s$ , and  $J$  have sharp maxima at frequencies divisible by the main frequency. The highest peak in Figures 8-10 cor-

responds to the main oscillation frequency of the shock. The other peaks correspond to higher harmonics due the oscillations being anharmonic.

We also investigated the stable regime of the radiative shock wave (case IV). To study the damping of the oscillations we introduced a small (10%) perturbation of the velocity in the upstream flow during a limited time. We used the “real” radiative function, and parameters as shown in the Table for case IV. One can see that when perturbations reached the front of the shock wave, the shock wave began to oscillate. However, these oscillations damped during several periods and stationary flow was re-established. Figure 11 shows an example of such damping.

## 8. CONCLUSIONS

This work has studied the stability/instability of the radiative MHD shock waves in the funnel streams of classical T Tauri stars. Matter flowing to the surface of the star along the magnetic field is decelerated in the radiative shock wave. The shock may be stable or unstable. In the case of instability the shock position and other variables oscillate and this can give observable short time-scale variability in the emitted radiation. A significant new aspect of the present work is that the magnetic field and the flow velocity parallel to it can have an arbitrary angle with respect to the normal to the star’s surface.

The shock wave has been modeled by solving the time-dependent MHD equations in one dimension (perpendicular to the star’s surface) taking into account the radiative losses. For the radiative losses we used either the “real” radiative function, approximated by segments of power laws (RTV) or by the power law function proposed by GS07.

Results of modelling of the radiative shock waves show that there is a simple criterion of the shock stability:  $3.7\sigma + 1.4\sin \chi > 1$ . This is for the case where the inflow to the shock is  $v_{\text{in}} \cos \chi = 1.3 \times 10^7 \text{cm s}^{-1}$ . We believe that this criterion will not change significantly at larger inflow velocities.

Comparison of the simulation results with the “real” (RTV) and power-law (GS) radiative functions shows that the qualitative results are similar. However, the periods of oscillations are significantly different.

The periods of oscillations are of the order of hundredths of a second for  $v_{\text{in}} \cos \chi = (1.3 - 3.0) \times 10^7 \text{cm s}^{-1}$ . This period is expected to increase with  $v_{\text{in}}$ . We estimate that  $P \approx 6 \times 10^{-3} [(v_{\text{in}} \cos \chi)/(10^7 \text{cm s}^{-1})]^3 \text{s}$ . The period of the oscillations varies,  $P = 0.02 - 0.2$ , depending on parameters.

Global three-dimensional simulations of magnetospheric accretion through the funnel streams have shown that hot spots on the surface of the star are *not homogeneous*: most of the kinetic energy flows in the central regions of the funnel stream so that the central regions of the spots are expected to be hotter (and also denser) compared to peripheral regions (Romanova et al. 2004; Kulkarni & Romanova 2005). Romanova et al. (2004) have shown that the spots may have very small filling factor at highest density and temperature (less than 1%) and much larger filling factor at smaller densities and temperatures (see Fig. 3 of Romanova et al. 2004). This fact has been recently confirmed observationally by Günther et al. (2007) who have shown that the filling factor in X-ray is smaller compared with

UV and optical bands which confirmed the inhomogeneity of the hot spots. Future research should be done for analysis of the stability of the global shock wave which would cover a significant part of the hot spot (not a small part as usually considered including this paper).

If the magnetic field near the star has a complex geometry (e.g. Valenti & Johns-Krull 2004; Gregory et al. 2006; Donati et al. 2007; Long, Romanova & Lovelace 2007, 2008), then it is likely that some field lines are inclined to the surface of the star as considered in this paper. The present analysis is thus applicable to the stability/instability of the shocks. If the complex field has significant transverse component then it may suppress oscillations.

Kravtsova & Lamzin (private communication) searched for oscillations of the shock in RW Aur using Crimean Observatory facilities. They did not find oscillations, though their time-resolution was low ( $\Delta P = 0.5 - 1$ s). They concluded that in this star there are no oscillations with periods  $P > 2$ s with amplitudes  $> 5\%$  above the noise level. Higher time-resolution observations in a larger sample of CTTs are needed to obtain a conclusive answer. It would

be useful to have high (ms) time-resolution observations in the UV and X-ray bands in stars with high veiling, such as RW Aur and others, because these wavebands would correspond to oscillations of the central part of the hot spots (Romanova et al. 2004; Günter et al. 2007) which may go into global oscillation mode with higher probability compared to peripheral parts observed in the optical band. A search in the optical band may bring interesting results as well because we do not know the details of the interaction of the funnel stream with a star on a global scale of the size of hot spot. To understand such physics, observations of variability time-scales would be informative and may help to shed a light to process of the funnel-star interaction.

#### ACKNOWLEDGEMENTS

Authors thank Dr. Lamzin and Dr. Beskin for helpful discussions and an anonymous referee for multiple questions and comments which improved the paper. This work has been partially supported by the NSF grants AST-0507760 and AST-0607135, and NASA grants NNG05GG77G and NAG5-13060. A.V.K. and G.V.U. were partially supported by RFBR grant 06-02-16608.

#### REFERENCES

- Ardila, D., & Basri, C. 2000, ApJ, 539, 834  
 Bertschinger E. 1986, ApJ, 304, 154  
 Bessolaz, N., Zanni, C., Ferreira, J., Keppens, R., Bouvier, J. 2008, A&A, 478, 155  
 Calvet, N., Gullbring, E. 1998, ApJ 509, 802  
 Canalle, J. B. G., Saxton, C. J., Wu, K., Cropper, M., Ramsay, G. 2005, A&A, 440, 185  
 Chevalier R.A., Imamura J.N. 1982, ApJ, 261, 543  
 Gnat O., Sternberg A. 2007, ApJ SS, 168, 213 (GS07)  
 Gregory, S.G., Jardine, M., Simpson, L., Donati, J.-F. 2006, MNRAS 371, 999  
 Cropper et al 1999 MNRAS 306, 664  
 Gullbring, E., Calvet, N., Muzerolle, J., Hartmann, L. 2000, ApJ, 544, 927  
 Günther, H.M., Schmitt, J.H.M.M., Robrade, J., & Liefke 2007, A&A, 466, 1111  
 Günther, H.M., & Schmitt, J.H.M.M., 2008, arXiv:0801.2273v2  
 Imamura, J.N., Aboasha, A., Wolff, M.T., Wood, K.S. 1996 ApJ 458, 327  
 Kulikovskii, A.G., Pogorelov, N.V., & Semenov, A.Yu. 2000, *Mathematical Aspects of Numerical Solution of Hyperbolic Systems*, Publisher: Chapman & Hall/CRC  
 Langer S., Chanmugan G., Shaviv G. 1981, ApJ, 245, L23  
 Lamzin, S.A. 1995, A&A, 295, L20  
 Lamzin, S.A. 1998, Astron. Reports 42, 322  
 Long M., Romanova M.M., Lovelace R.V.E. 2005, ApJ, 634, 1214  
 Long, M., Romanova, M.M. & Lovelace, R.V.E. 2007, MNRAS  
 Long, M., Romanova, M.M. & Lovelace, R.V.E. 2008, MNRAS, arXiv:0802.2308  
 Mignone A. 2005, ApJ, 626, 373  
 Peres G., Rosner R., Serio S., Vaiana G.S. 1982, ApJ, 252, 791  
 Ramachandran B., Smith M.D. 2005, MNRAS, 357, 707  
 Ramachandran B., Smith M.D. 2005, MNRAS, 362, 1353 (RS05)  
 Ramachandran B., Smith M.D. 2006, MNRAS, 366, 586  
 Raymond J.C., Smith B.W. 1977, ApJ SS, 35, 419  
 Romanova M.M., Ustyugova G.V., Koldoba A.V., Lovelace R.V.E. 2002, ApJ, 578, 420  
 Romanova M.M., Ustyugova G.V., Koldoba A.V., Lovelace R.V.E. 2004, ApJ, 610, 920  
 Rosner R., Tucker W.H., Vaiana G.S. 1978, ApJ, 220, 643  
 Saxton, C.J. 1998, MNRAS 299, 862  
 Saxton, C.J. 2002, PASA, 19, 282  
 Smith, K.W., Jones, D.H.P., & Clarke, C.J. 1996, MNRAS, 282, 167  
 Smith M.D. 1989, MNRAS, 238, 235  
 Smith M.D. 1993, AA, 272, 571  
 Smith, K.W., Jones, D.H.P., & Clarke, C.J. 1996, MNRAS, 282, 167  
 Spitzer, L. 1968, *Diffuse Matter in Space*, Interscience Pub.: New York, ch. 2  
 Strickland, R. & Blondin, J.M. 1995, ApJ 449, 727  
 Sutherland, R.S., Bicknell, G.V., Dopita, M.A. 2003, ApJ 591, 238  
 Toth G., Draine B.T. 1993, ApJ, 413, 176 (TD93)  
 Valenti, J.A., & Johns-Krull, C.M. 2004, Ap& SS, 292, 619